Published in final edited form as:
*Neuron*. 2013 October 16; 80(2): 350–357. doi:10.1016/j.neuron.2013.08.007.

# Subthreshold mechanisms underlying state-dependent modulation of visual responses

**Corbett Bennett**[*], **Sergio Arroyo**[*], and **Shaul Hestrin**[†]
Department of Comparative Medicine, Stanford University School of Medicine, Stanford, CA 94305, USA

## Summary

The processing of sensory information varies widely across behavioral states. However, little is known about how behavioral states modulate the intracellular activity of cortical neurons to effect changes in sensory responses. Here, we performed whole-cell recordings from neurons in upper-layer primary visual cortex of awake mice during locomotion and quiet wakefulness. We found that the signal-to-noise ratio for sensory responses was improved during locomotion by two mechanisms: (1) a decrease in membrane potential variability leading to a reduction in background firing rates, and (2) an enhancement in the amplitude and reliability of visually-evoked subthreshold responses mediated by an increase in total conductance and a depolarization of the stimulus-evoked reversal potential. Consistent with the enhanced signal-to-noise ratio for visual responses during locomotion, we demonstrate that performance is improved in a visual detection task during this behavioral state.

## Introduction

Nearly a century ago it was first observed that global brain activity, measured by electroencephalography (EEG), exhibits distinct electrical patterns corresponding to overt behavioral states (e.g. sleep, relaxation, alertness) (Berger, 1929; Loomis et al., 1935). Several studies have demonstrated that subthreshold activity can be tightly correlated with specific behavioral states. For example, intracellular recordings during slow wave sleep have shown that the membrane potential of cortical neurons exhibits slow (<1 Hz, “up/down”) fluctuations that are suppressed during wakefulness (Steriade et al., 2001). Moreover, recent findings suggest that wakefulness itself may comprise multiple states characterized by distinct membrane potential dynamics (Crochet and Petersen, 2006; Okun et al., 2010; Poulet and Petersen, 2008). In mouse barrel cortex, periods of quiet wakefulness are associated with large-amplitude, correlated fluctuations in membrane potential that are attenuated during active whisking (Crochet and Petersen, 2006; Poulet and Petersen, 2008). These studies raise the possibility that distinct membrane potential dynamics may mediate state-dependent modes of sensory processing.

Recent studies in mouse primary visual cortex (V1) have demonstrated that a particular behavioral state, locomotion, is correlated with increased responses to visual stimuli (Ayaz



[†]to whom correspondence should be addressed: shestrin@stanford.edu.
[*]these authors contributed equally to this manuscript

et al., 2013; Keller et al., 2012; Niell and Stryker, 2010). However, although these studies show a clear impact of behavioral state on spiking responses, the cellular mechanisms underlying these effects are poorly understood. To identify the processes that affect neuronal responses during different behavioral states, it is important to study the membrane potential dynamics preceding the generation of action potentials in individual neurons (Petersen and Crochet, 2013; Steriade et al., 2001).

To accomplish this, we performed whole-cell recordings from visual cortex in head-fixed mice allowed to run freely on a spherical treadmill (Dombeck et al., 2007). This approach allowed us to compare subthreshold cortical activity during two behavioral states: quiet wakefulness and locomotion. We found that locomotion was correlated with decreased membrane potential variability and an increase in the subthreshold response to visual stimulation. Together, these changes enhanced the neuronal signal-to-noise ratio during locomotion. Importantly, locomotion was also correlated with improved performance on a visual detection task, suggesting that the intracellular dynamics during quiet wakefulness and locomotion may impact visual perception.

## Results

### Behavioral state modulates spontaneous membrane potential dynamics

To determine whether locomotion and quiet wakefulness are associated with distinct membrane potential dynamics in V1 cortical neurons, we performed whole-cell recordings from upper-layer cortical cells in head-fixed mice during presentation of a uniform grey screen (Figure 1A). We defined quiet wakefulness as epochs for which the mean speed was < 0.5 cm/s, and locomotion as epochs for which the mean speed was > 1 cm/s, similar to thresholds used previously (Ayaz et al., 2013; Niell and Stryker, 2010). Eye movements were more frequent during locomotion and typically along the horizontal axis; however, the distributions of eye positions for the two states were highly overlapping and centered on a common default position (Supplemental Figure 1). During quiet wakefulness, cortical neurons displayed large-amplitude (~20 mV), low frequency (2–10 Hz) fluctuations that were attenuated during locomotion (Figure 1B–E; Supplemental Movie). To quantify this effect, we computed the variance in the membrane potential and the power in the 2–10 Hz frequency band for stationary and moving epochs (Figure 1D, F–H). During locomotion, the membrane potential was less variable and power in the 2–10 Hz band was diminished by a factor of two (Figure 1G–H; Table 1). Interestingly, the membrane potential dynamics of V1 neurons during stationary and moving periods were qualitatively similar to those observed during quiet wakefulness and active whisking in the barrel cortex (Crochet and Petersen, 2006; Crochet et al., 2011; Poulet et al., 2012), suggesting that high- and low-variance membrane potential dynamics may reflect general brain states conserved across sensory cortices.

### Spontaneous spiking during locomotion

The average membrane potential during locomotion was moderately depolarized relative to stationary periods (Figure 1I; Table 1). However, despite this depolarization, spontaneous firing rates were suppressed during locomotion (Figure 1J; Table 1). We next investigated the mechanisms that underlie this decrease in spontaneous spiking. It has been shown that spike threshold is sensitive to both the mean and the derivative of the membrane potential preceding spike generation (Azouz and Gray, 2000, 2003). Given the large-amplitude membrane potential fluctuations during quiet wakefulness, we hypothesized that the increase in spiking during stationary periods may reflect a hyperpolarization of the spike threshold. To compare the membrane potential dynamics preceding spike generation during stationary and moving epochs, we computed average spike waveforms for the two conditions (Figure

2A). As reported previously in anesthetized animals (Azouz and Gray, 2000, 2003), we found that spike threshold was negatively correlated with the derivative of the membrane potential ($dV_m/dt$) over the 10 ms preceding the spike (Figure 2B; $r_{stat}= -0.56$, $p_{stat} < 0.005$; $r_{mov}= -0.39$, $p_{mov} < 0.005$). However, although the membrane potential 100 ms before spike generation was significantly more hyperpolarized during stationary epochs (Figure 2C), $dV_m/dt$ was similar (Figure 2D), leading to nearly identical spike thresholds for the two conditions (Figure 2E). Furthermore, the maximum rate of rise during the action potential, a measure of the number of available voltage-gated sodium channels (Azouz and Gray, 2000), was not different for stationary and moving epochs (Table 1). These results suggest that the increased spiking during stationary epochs does not reflect a difference in intrinsic excitability between the two states.

We next tested whether the high variance membrane potential dynamics during stationary epochs could produce more frequent spike-threshold crossings without reducing the threshold itself. Indeed, we found that the probability of both hyperpolarized and depolarized membrane potentials was higher for the stationary state (Figure 2F). To quantify this observation, we measured the probability that the membrane potential was within 5 mV of spike threshold (probability near threshold, PNT) for stationary and moving epochs. For all cells tested, PNT was reduced during locomotion (Figure 2G; Supplemental Figure 2; Table 1). Moreover, PNT was well correlated with the change in spike rate between the two conditions (Figure 2H; $r = 0.87$, $p < 0.05$). Together, these findings suggest that the large-amplitude membrane potential fluctuations during stationary epochs increase spiking, not by modulating intrinsic excitability, but by increasing the fraction of time during which the membrane potential is near spike threshold.

## Behavioral state modulates subthreshold visually-evoked responses

Several recent studies using extracellular recordings (Ayaz et al., 2013; Niell and Stryker, 2010) and calcium imaging (Keller et al., 2012) have demonstrated that locomotion increases visually-evoked spiking in mouse V1. To verify that visually-evoked firing rates were similarly enhanced during locomotion for our experimental setup, we performed juxtacellular recordings and measured the response of each cell to a brief (83 ms) flash of optimally-oriented gratings (Supplemental Figure 3A). Maximum responses to flashed gratings were consistently higher for moving than for stationary periods (Supplemental Figure 3B, C; Table 1). We calculated the number of standard deviations that the maximum visual response rose above baseline for both behavioral states (z-score). The increase in response firing during locomotion, together with a decrease in background firing (Figure 1J, SU symbols), led to significantly higher z-scores for the visual response during locomotion (Supplemental Figure 3D; Table 1).

What intracellular mechanisms mediate the increase in stimulus-evoked spiking during locomotion? In principle, the mean depolarization during locomotion (Figure 1I) could produce higher stimulus-evoked firing with or without a concomitant change in the response amplitude. To test these possibilities, we recorded subthreshold responses to optimally-oriented drifting sinusoidal gratings (16% contrast, ~1.2 s) during stationary and moving epochs (Figure 3A). To better isolate subthreshold responses to visual stimulation, we suppressed the generation of action potentials by injecting hyperpolarizing current (resulting $V_m$: $-82.7 \pm 4.1$ mV). We found that the amplitude of the response, averaged over the entire stimulus window, was significantly larger during locomotion (Figure 3B, E; Table 1). Indeed, in several cases (3/8), the visual response was only measurable during locomotion.

To examine whether behavioral state modulates response variability, we calculated trial-to-trial correlations in the visual response for stationary and moving epochs. We observed a striking reduction in response variability during locomotion (Figure 3C), manifested as an

increase in the mean correlation coefficient between trials (Figure 3D, E; Table 1). Additionally, the coefficient of variation (CV), computed for the peak response following the initial visual transient, was significantly reduced during moving epochs (Figure 3E; Table 1). Together, these metrics indicate that both the waveform and the amplitude of the visual response were more reliable during locomotion.

The response to visual stimulation consists of excitatory and inhibitory inputs (Borg-Graham et al., 1998; Haider et al., 2006; Haider et al., 2013; Haider et al., 2010; Isaacson and Scanziani, 2011; Liu et al., 2010; Priebe and Ferster, 2005; Tan et al., 2011), and the increased visual response during locomotion might reflect changes in either or both of these conductances. To investigate the changes in excitatory ($g_e$) and inhibitory ($g_i$) conductances measured at the soma, we recorded intracellular responses to drifting sinusoidal gratings (100% contrast) under voltage clamp. Using a $Cs^+$-based internal solution, we recorded visually-evoked currents while maintaining the cell's membrane at two holding potentials, +20 and −70 mV, to calculate $g_e$ and $g_i$ (see Experimental Procedures). Under these conditions, locomotion was correlated with an increase in both $g_e$ and $g_i$ for all cells tested (Figure 3F, G; Table 1). Interestingly, the balance of excitation and inhibition (E/I balance) was also modulated by behavioral state, reflected by a depolarization in the reversal potential of the visually-evoked conductances (Figure 3H; Table 1). Together, both an increase in total conductance and a shift in the E/I balance towards excitation would be expected to produce larger subthreshold depolarizations, consistent with our current clamp data and the increased spiking during locomotion reported here and in previous studies (Supplemental Figure 2; Ayaz et al., 2013; Niell and Stryker, 2010).

### Visual detection is improved during locomotion

To examine whether the stationary and moving states are relevant for visual behavior, we trained mice to perform a visual detection task and analyzed their performance during the two conditions. Mice learned to lick for a water reward during the presentation of drifting gratings of varying contrasts (low: 9/16%; medium: 27/50%; high: 81/100%) and to withhold licking for the presentation of a grey screen (Figure 4A, B; Supplemental Figure 4A, B). Injection of the $GABA_A$-receptor agonist muscimol into V1 (n=4) significantly impaired behavioral performance compared to saline controls (n=4; Figure 4C; Supplemental Figure 4C), indicating that the visual cortex was necessary for this task.

Interestingly, locomotion was correlated with a significant increase in the hit rates for both low and medium contrast gratings. False alarm rates also increased during locomotion, though this effect was driven primarily by one animal and did not reach significance (Figure 4D; Table 2). An increase in hit rates could reflect an overall increase in licking and not improved perception. To distinguish between these possibilities, we computed the discriminability ($d'$) for each contrast (Figure 4E; Table 2), a metric that is invariant to the behavioral criterion (Wickens, 2002). For each mouse tested, $d'$ was enhanced during locomotion for the low contrast condition; however, no significant effect was observed for the medium and high contrast conditions, likely reflecting a saturation of performance (Figure 4F; Table 2). Notably, moving trials were evenly distributed across the entire behavioral session (Supplemental Figure 4D), and performance during the first and second halves of the sessions did not differ ($p > 0.1$, Wilcoxon signed-rank test). Thus, the improvement in $d'$ during movement did not reflect a correlation between locomotion and motivation.

## Discussion

Here we present three main findings. First, we show large-amplitude, low-frequency membrane potential fluctuations in V1 during quiet wakefulness that are abolished during

locomotion. This decrease in membrane potential variability results in reduced spontaneous firing rates during locomotion. Second, we demonstrate that locomotion was correlated with an increase in both the amplitude and reliability of the subthreshold response to visual stimuli. This enhanced response was mediated by an increase in visually-evoked excitatory and inhibitory conductance and a shift in the E/I balance towards excitation. Finally, we show that locomotion is correlated with improved performance in a visual detection task, as might be predicted from our physiological results. Together these findings provide intracellular mechanisms for state-dependent improvement in sensory coding in the awake animal.

### Low frequency fluctuations in cortical neurons

Synchronous, low frequency activity during quiescence and sleep have long been observed by EEG and local field potential (LFP) recordings. However, the connection between these measurements of brain activity and intracellular dynamics has only recently been explored (Crochet and Petersen, 2006; Okun et al., 2010; Poulet and Petersen, 2008; Steriade et al., 2001). To date, high-variance membrane potential fluctuations during wakefulness have only been reported in the barrel cortex, where they emerge during periods of quiet wakefulness, i.e. when the animal is not actively whisking. Given the established role of the barrel cortex in not only sensing but also generating whisker movements (Matyas et al., 2010), it was unclear whether these dynamics were a unique feature of the rodent whisker system. However, by extending these findings to another sensory cortex, our data suggest that high and low variance membrane potential dynamics may represent distinct sensory processing modes, conserved across diverse brain areas.

### State-dependent enhancement in sensory processing

A recent study has shown that locomotion is correlated with both a reduction in low-frequency power in the LFP and enhanced visual responses (Niell and Stryker, 2010). Here we report a similar enhancement in spiking responses during locomotion and uncover the cellular mechanisms that underlie this effect. Specifically, we demonstrate that subthreshold visual responses are larger and more reliable during locomotion due to an increase in excitatory and inhibitory conductance and a depolarization in the visually-evoked reversal potential.

It has been suggested that the brain state observed during locomotion and other active behaviors in the rodent (Crochet and Petersen, 2006; Niell and Stryker, 2010; Okun et al., 2010) may be analogous to the brain state observed in primates during selective attention (Harris and Thiele, 2011). While the increase in firing rate and reduction in trial-to-trial reliability during attention are well-established (Noudoost et al., 2010), the cellular mechanisms underlying these effects are not known. We propose that an increase in synaptic conductance, a shift in the E/I balance, and a reduction in spontaneous membrane potential variability may represent general principles that contribute to enhanced sensory coding, not only during locomotion, but in a wide variety of behavioral states including attention.

We argue that the signal-to-noise ratio for sensory responses during locomotion is improved in part by a decrease in spontaneous firing. A number of other studies using extracellular recordings have reported a similar reduction in spontaneous firing during desynchronized brain states (Livingstone and Hubel, 1981; Sakata and Harris, 2012). Here, we extend these findings by showing that this decrease in spiking results from a reduction in membrane potential variance and not a state-dependent modulation of intrinsic excitability. Given that the effect of desynchronized states on spiking activity may depend on laminar position and cell-type identity (de Kock and Sakmann, 2009; Gentet et al., 2010; Gentet et al., 2012;

Sakata and Harris, 2012), it will be interesting to investigate how the subthreshold dynamics we report here vary across different classes of neurons.

Notably, the decrease in spontaneous spiking during locomotion that we report here was not observed in three recent studies in mouse visual cortex, likely reflecting differences in experimental design (Ayaz et al., 2013; Keller et al., 2012; Niell and Stryker, 2010). Niell and Stryker report no change in spontaneous spiking during locomotion; however, they measure spontaneous activity during relatively brief intervals between visual stimuli, and thus their estimates may be influenced by previous visual responses. Keller et al. report increased $Ca^{2+}$ signals during locomotion; however, as the authors note, their data is likely biased towards cells with high firing rates and strong $Ca^{2+}$ signals, a class of cells that we may not sample at the same rate. Finally, Ayaz et al. report an increase in spontaneous firing during locomotion. However, they record primarily from the lower layers (L4 and L5), where state-dependent modulation of spontaneous activity may differ.

Importantly, we demonstrate that both the balance of excitation and inhibition and the total conductance for sensory responses depend on behavioral state. This finding represents a divergence from the canonical view that excitation and inhibition are recruited proportionally (Isaacson and Scanziani, 2011). Though we used a $Cs^{+}$-based internal solution and analyzed only time-averaged conductances, the visually-evoked conductances we report here are undoubtedly underestimates of the true conductances due to poor dendritic space clamp (Williams and Mitchell, 2008). However, though the absolute magnitudes of excitatory and inhibitory conductances are sensitive to poor space clamp, the relative shift in the balance of excitation and inhibition between behavioral states is less likely to reflect this error.

How might behavioral state uncouple excitatory and inhibitory conductances? It has been shown that neuromodulators such as noradrenaline and acetylcholine may impact cortical processing by targeting specific cell-types and synapses (Kawaguchi and Shindou, 1998; Picciotto et al., 2012). For example, by activating inhibitory interneurons, noradrenaline might shift inhibitory synapses into a state of synaptic depression, limiting feedforward inhibition in response to sensory stimuli (Kawaguchi and Shindou, 1998; Kuo and Trussell, 2011). Additionally, acetylcholine has been shown to enhance the efficacy of thalamocortical synapses onto excitatory cells while suppressing local inhibitory synapses (Disney et al., 2007; Gil et al., 1999; Kruglikov and Rudy, 2008). Given that putative cholinergic and noradrenergic projection neurons exhibit increased firing rates during movement (Buzsaki et al., 1988) and behavioral state transitions (Aston-Jones and Bloom, 1981), respectively, it is possible that these ascending neuromodulatory systems may contribute to the state-dependent modulation of visually-evoked conductances shown here.

## Functional Implications

What is the function of high- and low-variance brain states? The prevalence of slow, synchronous activity in EEG recordings during contemplative or internally-directed mental states (Schacter, 1977) suggests that low frequency fluctuations may facilitate intracortical interactions. Indeed, a recent study demonstrated that cortical replay of a learned sensory sequence was enhanced during periods of quiet wakefulness, when the LFP power was concentrated in the low frequency band (Xu et al., 2012). By coordinating spiking in discrete temporal windows, low frequency fluctuations could magnify postsynaptic responses and facilitate spike-timing-dependent plasticity.

Conversely, by suppressing fluctuations that are not synchronized with sensory-evoked activity, the low-variance state could improve the fidelity of sensory representations. Indeed, we found that both the amplitude and the waveform of visual responses were more reliable

during the low-variance state. Such an improvement in sensory coding might be important during sensory-guided behaviors that depend on an efficient and reliable response to environmental stimuli.

## Experimental Procedures

### Animals and surgery

All procedures were approved by the Administrative Panel on Laboratory Animal Care at Stanford University. Headplates were centered over V1 on the left hemisphere, and mice were given at least 2 days to recover before habituation to the spherical treadmill(~3 days).

### In vivo recording

A <200 μm craniotomy was made over monocular V1, and recordings were obtained using standard blind patching techniques. Only recordings at a depth of less than 400 μm were included in this study. All recordings were corrected for a junction potential of −10 mV.

### Visual Stimulation

Visual stimuli were presented on gamma-corrected LED monitors (60 Hz refresh rate, ~75 $cd/m^2$) placed 30 cm from the mouse and subtending ~90 degrees of visual space. Stimuli were full-screen sinusoidal gratings (0.05 cycles/degree, 40°/second).

### Data analysis

Moving and stationary epochs were identified as periods during which the speed was greater than 1 cm/s and less than 0.5 cm/s, respectively. Membrane potential power spectra, resting potential, spike rate, and membrane potential variance were calculated for 500 ms segments and averaged to obtain stationary and moving values. For current clamp experiments in Figure 3, response amplitude and trial-to-trial correlations were calculated over the entire stimulus window (~1.2 s duration). The coefficient of variation was calculated for a 100 ms window centered on the mean response peak after the initial visual transient. For voltage clamp experiments in Figure 3, visual responses were recorded at +20 mV and −70 mV, and $g_e$ and $g_i$ were calculated over the stimulus window (see Supplemental Experimental Procedures).

All paired statistical comparisons were performed with the non-parametric Wilcoxon signed-rank test. Non-paired comparisons were performed with the non-parametric Wilcoxon rank-sum test. All analysis was performed in Matlab.

### Behavior

To categorize behavioral trials as stationary or moving, we analyzed the 500 ms before stimulus onset. Data from six behavioral sessions were combined and analyzed. The cortical inactivation experiment was performed over four days. Baseline performance was measured over the first two days, a craniotomy was performed on the third day, and either muscimol (4.4 mM; ~400 nL) or saline was injected on the fourth day (saline cohort: n=4; muscimol cohort: n=4). Performance was normalized to the mean performance on days 1 and 2.

## Supplementary Material

Refer to Web version on PubMed Central for supplementary material.

## Acknowledgments

We would like to thank Xiaoting Wang for helping to train mice on the visual detection task. We would also like to thank Chris Niell and Michael Stryker for advice on the experimental setup. This work was supported by the NIH (EY012114 to S.H., Ruth L. Kirschstein Graduate Fellowship and the Medical Scientist Training Program to S.A.) and the NSF (Graduate Research Fellowship Program to C.B.).

## References

Aston-Jones G, Bloom FE. Activity of norepinephrine-containing locus coeruleus neurons in behaving rats anticipates fluctuations in the sleep-waking cycle. The Journal of neuroscience : the official journal of the Society for Neuroscience. 1981; 1:876–886. [PubMed: 7346592]

Ayaz A, Saleem AB, Scholvinck ML, Carandini M. Locomotion controls spatial integration in mouse visual cortex. Current biology : CB. 2013; 23:890–894. [PubMed: 23664971]

Azouz R, Gray CM. Dynamic spike threshold reveals a mechanism for synaptic coincidence detection in cortical neurons in vivo. Proceedings of the National Academy of Sciences of the United States of America. 2000; 97:8110–8115. [PubMed: 10859358]

Azouz R, Gray CM. Adaptive coincidence detection and dynamic gain control in visual cortical neurons in vivo. Neuron. 2003; 37:513–523. [PubMed: 12575957]

Berger H. Über das elektrenkephalogramm des menschen. European Archives of Psychiatry and Clinical Neuroscience. 1929; 87:527–570.

Borg-Graham LJ, Monier C, Fregnac Y. Visual input evokes transient and strong shunting inhibition in visual cortical neurons. Nature. 1998; 393:369–373. [PubMed: 9620800]

Buzsaki G, Bickford RG, Ponomareff G, Thal LJ, Mandel R, Gage FH. Nucleus basalis and thalamic control of neocortical activity in the freely moving rat. The Journal of neuroscience : the official journal of the Society for Neuroscience. 1988; 8:4007–4026. [PubMed: 3183710]

Crochet S, Petersen CC. Correlating whisker behavior with membrane potential in barrel cortex of awake mice. Nature neuroscience. 2006; 9:608–610.

Crochet S, Poulet JF, Kremer Y, Petersen CC. Synaptic mechanisms underlying sparse coding of active touch. Neuron. 2011; 69:1160–1175. [PubMed: 21435560]

de Kock CP, Sakmann B. Spiking in primary somatosensory cortex during natural whisking in awake head-restrained rats is cell-type specific. Proceedings of the National Academy of Sciences of the United States of America. 2009; 106:16446–16450. [PubMed: 19805318]

Disney AA, Aoki C, Hawken MJ. Gain modulation by nicotine in macaque v1. Neuron. 2007; 56:701–713. [PubMed: 18031686]

Dombeck DA, Khabbaz AN, Collman F, Adelman TL, Tank DW. Imaging large-scale neural activity with cellular resolution in awake, mobile mice. Neuron. 2007; 56:43–57. [PubMed: 17920014]

Gentet LJ, Avermann M, Matyas F, Staiger JF, Petersen CC. Membrane potential dynamics of GABAergic neurons in the barrel cortex of behaving mice. Neuron. 2010; 65:422–435. [PubMed: 20159454]

Gentet LJ, Kremer Y, Taniguchi H, Huang ZJ, Staiger JF, Petersen CC. Unique functional properties of somatostatin-expressing GABAergic neurons in mouse barrel cortex. Nature neuroscience. 2012; 15:607–612.

Gil Z, Connors BW, Amitai Y. Efficacy of thalamocortical and intracortical synaptic connections: quanta, innervation, and reliability. Neuron. 1999; 23:385–397. [PubMed: 10399943]

Haider B, Duque A, Hasenstaub AR, McCormick DA. Neocortical network activity in vivo is generated through a dynamic balance of excitation and inhibition. The Journal of neuroscience : the official journal of the Society for Neuroscience. 2006; 26:4535–4545. [PubMed: 16641233]

Haider B, Hausser M, Carandini M. Inhibition dominates sensory responses in the awake cortex. Nature. 2013; 493:97–100. [PubMed: 23172139]

Haider B, Krause MR, Duque A, Yu Y, Touryan J, Mazer JA, McCormick DA. Synaptic and network mechanisms of sparse and reliable visual cortical activity during nonclassical receptive field stimulation. Neuron. 2010; 65:107–121. [PubMed: 20152117]

Harris KD, Thiele A. Cortical state and attention. Nature reviews Neuroscience. 2011; 12:509–523.

Isaacson JS, Scanziani M. How inhibition shapes cortical activity. Neuron. 2011; 72:231–243. [PubMed: 22017986]

Kawaguchi Y, Shindou T. Noradrenergic excitation and inhibition of GABAergic cell types in rat frontal cortex. The Journal of neuroscience : the official journal of the Society for Neuroscience. 1998; 18:6963–6976. [PubMed: 9712665]

Keller GB, Bonhoeffer T, Hubener M. Sensorimotor mismatch signals in primary visual cortex of the behaving mouse. Neuron. 2012; 74:809–815. [PubMed: 22681686]

Kruglikov I, Rudy B. Perisomatic GABA release and thalamocortical integration onto neocortical excitatory cells are regulated by neuromodulators. Neuron. 2008; 58:911–924. [PubMed: 18579081]

Kuo SP, Trussell LO. Spontaneous spiking and synaptic depression underlie noradrenergic control of feed-forward inhibition. Neuron. 2011; 71:306–318. [PubMed: 21791289]

Liu BH, Li P, Sun YJ, Li YT, Zhang LI, Tao HW. Intervening inhibition underlies simple-cell receptive field structure in visual cortex. Nature neuroscience. 2010; 13:89–96.

Livingstone MS, Hubel DH. Effects of sleep and arousal on the processing of visual information in the cat. Nature. 1981; 291:554–561. [PubMed: 6165893]

Loomis AL, Harvey EN, Hobart G. Potential Rhythms of the Cerebral Cortex during Sleep. Science. 1935; 81:597–598. [PubMed: 17739875]

Matyas F, Sreenivasan V, Marbach F, Wacongne C, Barsy B, Mateo C, Aronoff R, Petersen CC. Motor control by sensory cortex. Science. 2010; 330:1240–1243. [PubMed: 21109671]

Niell CM, Stryker MP. Modulation of visual responses by behavioral state in mouse visual cortex. Neuron. 2010; 65:472–479. [PubMed: 20188652]

Noudoost B, Chang MH, Steinmetz NA, Moore T. Top-down control of visual attention. Current opinion in neurobiology. 2010; 20:183–190. [PubMed: 20303256]

Okun M, Naim A, Lampl I. The subthreshold relation between cortical local field potential and neuronal firing unveiled by intracellular recordings in awake rats. The Journal of neuroscience : the official journal of the Society for Neuroscience. 2010; 30:4440–4448. [PubMed: 20335480]

Petersen CC, Crochet S. Synaptic computation and sensory processing in neocortical layer 2/3. Neuron. 2013; 78:28–48. [PubMed: 23583106]

Picciotto MR, Higley MJ, Mineur YS. Acetylcholine as a neuromodulator: cholinergic signaling shapes nervous system function and behavior. Neuron. 2012; 76:116–129. [PubMed: 23040810]

Poulet JF, Fernandez LM, Crochet S, Petersen CC. Thalamic control of cortical states. Nature neuroscience. 2012; 15:370–372.

Poulet JF, Petersen CC. Internal brain state regulates membrane potential synchrony in barrel cortex of behaving mice. Nature. 2008; 454:881–885. [PubMed: 18633351]

Priebe NJ, Ferster D. Direction selectivity of excitation and inhibition in simple cells of the cat primary visual cortex. Neuron. 2005; 45:133–145. [PubMed: 15629708]

Sakata S, Harris KD. Laminar-dependent effects of cortical state on auditory cortical spontaneous activity. Frontiers in neural circuits. 2012; 6:109. [PubMed: 23267317]

Schacter DL. EEG theta waves and psychological phenomena: a review and analysis. Biological psychology. 1977; 5:47–82. [PubMed: 193587]

Steriade M, Timofeev I, Grenier F. Natural waking and sleep states: a view from inside neocortical neurons. Journal of neurophysiology. 2001; 85:1969–1985. [PubMed: 11353014]

Tan AY, Brown BD, Scholl B, Mohanty D, Priebe NJ. Orientation selectivity of synaptic input to neurons in mouse and cat primary visual cortex. The Journal of neuroscience : the official journal of the Society for Neuroscience. 2011; 31:12339–12350. [PubMed: 21865476]

Wickens, TD. Elementary signal detection theory. New York: Oxford University Press; 2002.

Williams SR, Mitchell SJ. Direct measurement of somatic voltage clamp errors in central neurons. Nature neuroscience. 2008; 11:790–798.

Xu S, Jiang W, Poo MM, Dan Y. Activity recall in a visual cortical ensemble. Nature neuroscience. 2012; 15:449–455. S441–442.

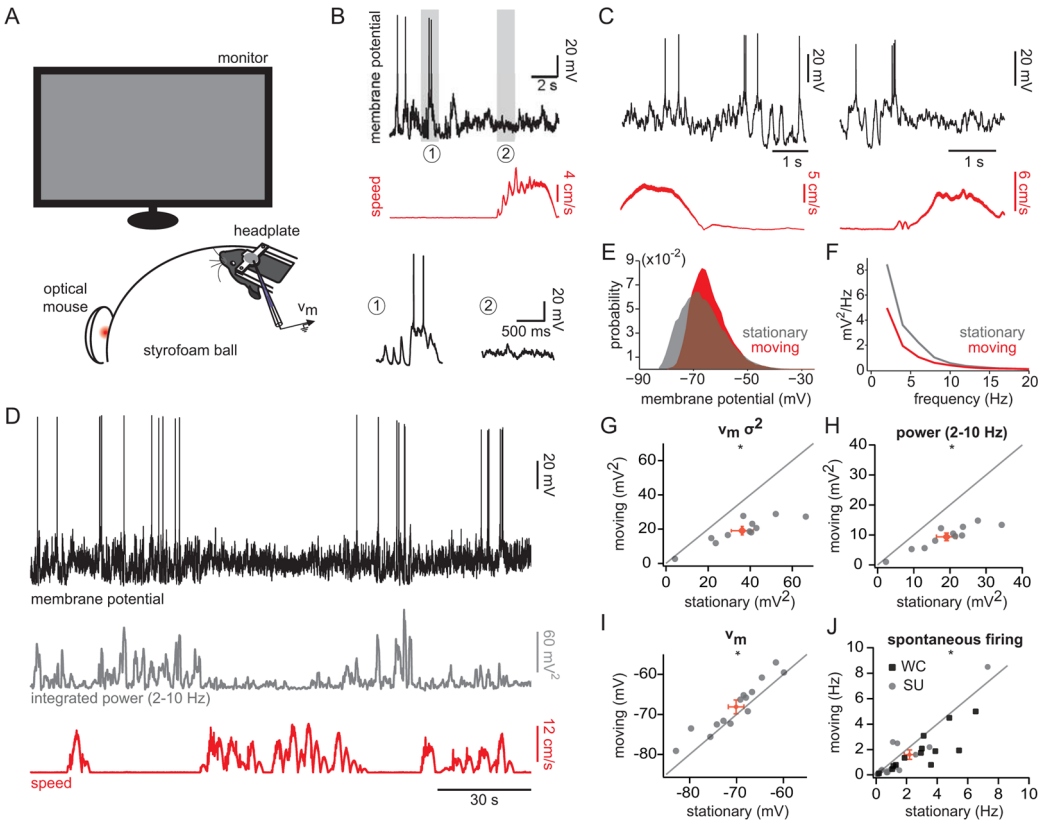


**Figure 1. Intracellular correlates of behavioral state in mouse visual cortex**

(A) Experimental set-up. (B) Membrane potential of a V1 neuron (top) and speed (middle). Bottom, insets of membrane potential during (1) stationary and (2) moving epochs. (C) Example membrane potential recordings and speed measurements for two additional neurons. (D) Membrane potential for cell in (B) (top) plotted with the integral of the power density function in the 2–10 Hz band (middle) and speed (bottom). (E) All-point histogram of membrane potential during stationary and moving states for cell in (B). (F) Power spectrum density for stationary and moving states for cell in (B). (G–J) Population plots for membrane potential variance (G), 2–10 Hz power (H), membrane potential (I), and spontaneous firing rate (J) for stationary and moving states. Grey and black symbols represent individual cells. Red symbols represent the mean ± SEM. WC: whole-cell; SU: single-unit. *, $p < 0.01$, Wilcoxon signed-rank test. See also Figure S1.

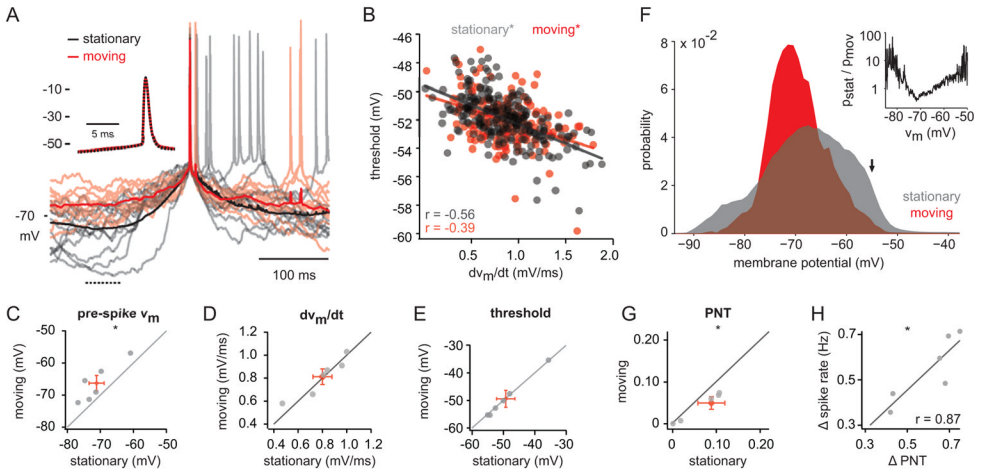


**Figure 2. Reduced spiking during movement reflects decreased variance and not change in spike threshold**

(A) Average action potential waveforms for stationary (black) and moving (red) epochs for a representative neuron. Light traces depict individual trials. Dotted line on bottom left denotes pre-spike interval used in (C). Inset: Expanded time scale. Black trace is dotted to reveal overlap between conditions. (B) Threshold for spikes during stationary (grey) and moving (red) epochs plotted against the mean $dV_m/dt$ during the 10 ms prior to spike initiation. Lines represent fits to the data. (C–E) Pre-spike $V_m$ (C), $dV_m/dt$ (D), and spike threshold (E) is plotted for moving vs. stationary epochs (n = 6 neurons). (F) All-point histogram of membrane potential during stationary and moving epochs for one neuron. Arrow denotes spike threshold. Inset: ratio of all-point histograms (stationary/moving) for stationary and moving epochs demonstrates relative likelihood of membrane potentials for the two conditions. (G) Probability near threshold (PNT) for stationary and moving epochs (n=6 neurons). (H) Difference in spike rate (stationary-moving) plotted against difference in PNT. Red symbols represent the mean ± SEM. *, $p < 0.05$; Wilcoxon signed-rank test. See also Figure S2.

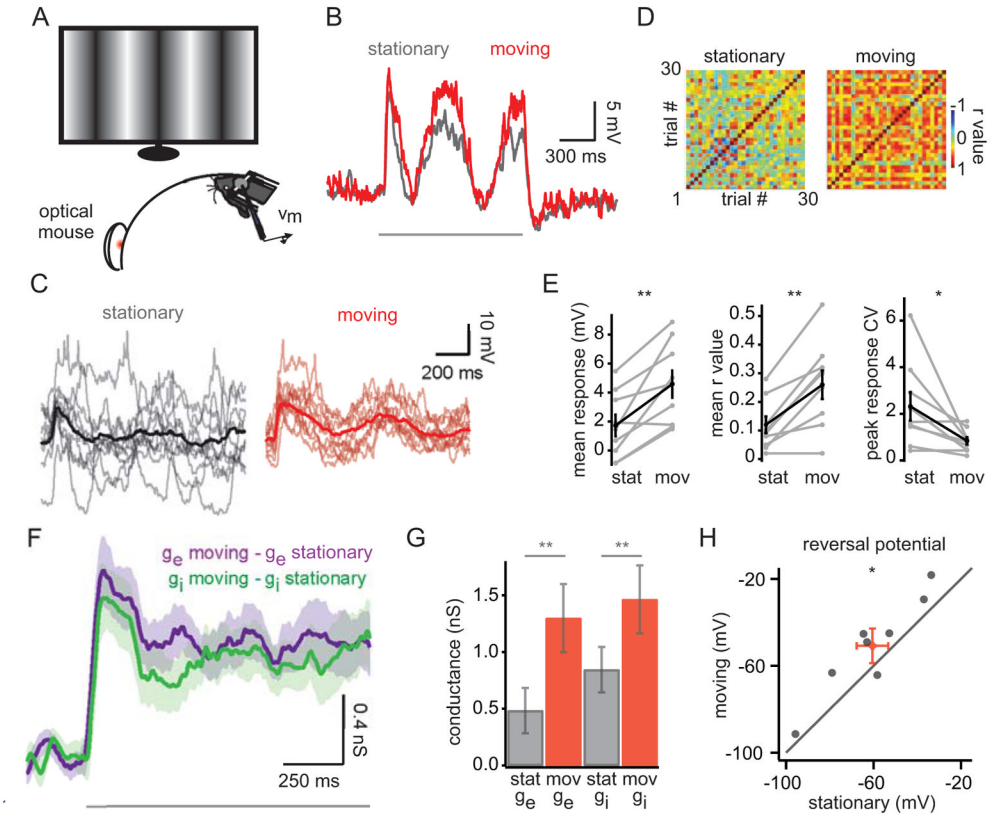


**Figure 3. Visual responses are larger and more reliable during movement**

(A) Experimental set-up. Drifting sinusoidal gratings were presented (16% contrast for current clamp recordings (B–E); 100% contrast for voltage clamp recordings (F–H); ~1.2 s grating presentation interleaved with ~3.8 s of grey screen). (B) Averaged visual response for one neuron for stationary (grey) and moving (red) states. Grey bar denotes stimulus presentation. (C) Single trial (light traces) and averaged responses (bold traces) for stationary and moving states for an example neuron. (D) Trial-to-trial correlation matrix of visual responses for stationary (left) and moving (right) states for the neuron in (C). (E) Mean stimulus response (averaged over the entire stimulus presentation), mean r value, and coefficient of variation (CV; calculated for the response peak) for population of neurons (n=9). (F) Difference in excitatory (purple) and inhibitory (green) conductances between stationary and moving states averaged across 10 neurons. Transparency represents SEM. (G) Mean $g_e$ and $g_i$ are depicted for the stationary and moving states. Values represent the mean across the stimulus window; error bars represent the SEM. (H) Reversal potential of the stimulus-evoked conductances for stationary and moving states (n=8). Red symbol represents the mean ± SEM. *, $p < 0.05$; **, $p < 0.01$ Wilcoxon signed-rank test. See also Figure S3.

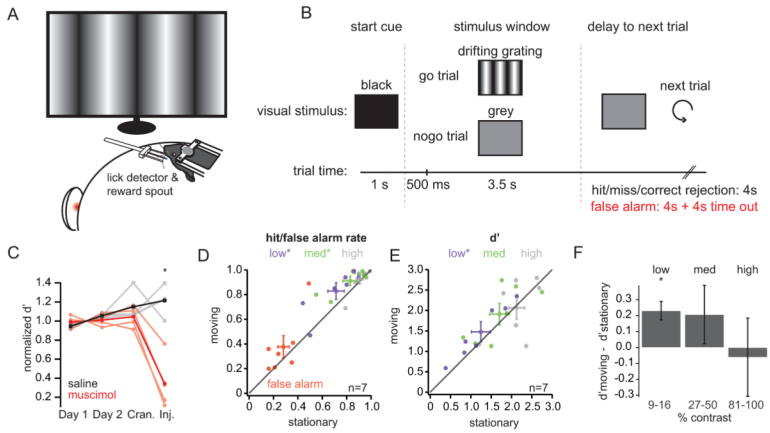


**Figure 4. Visual detection is improved during movement**

(A) Experimental set-up. (B) Behavioral paradigm. Trials began with a start cue (1s; black screen) followed by a stimulus window (4s; drifting gratings or grey screen). Licks during the first 500 ms of the stimulus window were neither punished nor rewarded. Following the stimulus presentation, there was an inter-trial period of either 4 seconds (for hit, miss, and correct rejection trials) or 8 seconds (for false alarm trials). (C) Normalized discriminability (d′) for two cohorts of mice receiving saline (grey traces, individual mice; black trace, average) or the $GABA_A$ agonist muscimol (light red traces, individual mice; red trace, average). Performance was normalized to mean d′ over days 1 and 2. Cran.: day of craniotomy; inj.: day of injection. (D) False alarm rates (red), low contrast hit rates (9–16% contrast; purple), medium contrast hit rates (27–50% contrast; green), and high contrast hit rates (81–100% contrast; grey) are plotted for stationary and moving states. Diamonds with error bars represent the mean ± SEM. (E) d′ for low, medium, and high contrasts plotted for stationary and moving states. Colors and symbols as in (D). (F) Difference in d′ for stationary and moving states averaged across seven mice. *, $p<0.05$, Wilcoxon signed-rank test. See also Figure S4.

**Table 1**

Summary of electrophysiological data

| | | Stationary | Moving | n | p | Figure |
|---|---|---|---|---|---|---|
| **Spontaneous activity** | Vm (mV) | −70.1 ± 1.7 | −68.1 ± 1.7 | 14 | 0.0032 | 1 |
| | Vm variance ($mV^2$) | 36.2 ± 5.2 | 19.1 ± 2.5 | 11 | 0.001 | 1 |
| | Power (2–10 Hz; $mV^2$) | 19.0 ± 2.7 | 9.4 ± 1.2 | 11 | 0.001 | 1 |
| | Spontaneous firing rate (Hz) | 2.2 ± 2.0 | 1.6 ± 1.9 | 28 | 0.0025 | 1 |
| | Spike threshold (mV) | −49.2 ± 2.9 | −49.4 ± 3.1 | 6 | 0.38 | 2 |
| | Pre-spike potential (mV) | −71.1 ± 2.3 | −66.3 ± 2.4 | 6 | 0.016 | 2 |
| | Pre-spike $dV_m/dt$ (mV/ms) | 0.80 ± 0.08 | 0.81 ± 0.07 | 6 | 0.81 | 2 |
| | Maximum spike $dV_m/dt$ (mV/ms) | 144.5 ± 3.0 | 143.8 ± 2.7 | 6 | 1 | 2 |
| | Probability near threshold (PNT) | 0.09 ± 0.03 | 0.05 ± 0.01 | 6 | 0.03 | 2 |
| **Stimulus-evoked activity** | Peri-stimulus firing rate (Hz) | 7.7 ± 2.0 | 12.6 ± 3.3 | 12 | 0.02 | S3 |
| | z-score | 16.2 ± 3.6 | 41.8 ± 11.8 | 12 | 0.02 | S3 |
| | Mean response amplitude (mV) | 1.7 ± 0.8 | 4.6 ± 0.9 | 9 | 0.008 | 3 |
| | Mean r value | 0.11 ± 0.03 | 0.26 ± 0.05 | 9 | 0.004 | 3 |
| | Coefficient of variation (peak) | 2.32 ± 0.6 | 0.8 ± 0.2 | 9 | 0.02 | 3 |
| | $g_e$ (nS) | 0.5 ± 0.2 | 1.3 ± 0.3 | 8 | 0.008 | 3 |
| | $g_i$ (nS) | 0.8 ± 0.2 | 1.5 ± 0.3 | 8 | 0.008 | 3 |
| | Reversal potential (peak; mV) | −60.5 ± 7.2 | −50.8 ± 8.0 | 8 | 0.02 | 3 |

**Table 2**

Summary of behavioral data

| | | Stationary | Moving | n | p | Figure |
|---|---|---|---|---|---|---|
| **Behavior** | False alarm rate | 0.28 ± 0.05 | 0.38 ± 0.09 | 7 | 0.19 | 4 |
| | High contrast hit rate | 0.91 ± 0.03 | 0.93 ± 0.04 | 7 | 0.31 | 4 |
| | Medium contrast hit rate | 0.83 ± 0.06 | 0.91 ± 0.04 | 7 | 0.047 | 4 |
| | Low contrast hit rate | 0.71 ± 0.07 | 0.83 ± 0.07 | 7 | 0.031 | 4 |
| | High contrast d′ | 2.1 ± 0.19 | 2.1 ± 0.28 | 7 | 1 | 4 |
| | Medium contrast d′ | 1.7 ± 0.24 | 1.9 ± 0.26 | 7 | 0.297 | 4 |
| | Low contrast d′ | 1.2 ± 0.23 | 1.5 ± 0.25 | 7 | 0.0156 | 4 |